Photometric and polarimetric studies towards NGC 1931

C. Eswaraiah, A. K. Pandey, S. Sharma, and Ram Kesh Yadav

Citation: AIP Conf. Proc. **1543**, 138 (2013); doi: 10.1063/1.4812608
View online: http://dx.doi.org/10.1063/1.4812608
View Table of Contents: http://proceedings.aip.org/dbt/dbt.jsp?KEY=APCPCS&Volume=1543&Issue=1
Published by the AIP Publishing LLC.

Photometric and polarimetric studies towards NGC 1931

C. Eswaraiah, A. K. Pandey, S. Sharma and Ram Kesh Yadav

Aryabhatta Research Institute of observational Sciences (ARIES), Naintal, INDIA

Abstract. We investigated the dust properties and magnetic field orientation towards the star cluster NGC 1931. Cluster members have been identified using both optical color-color as well as $Q_V - U_V$ stokes plane diagrams. Thus identified probable cluster members have been used to estimate the distance to the cluster NGC 1931 which is found to be 2.3±0.3 kpc. Few young stellar objects with possible intrinsic polarization have been identified. One-dimensional surface stellar density contours suggest two clustering in the NGC 1931 region. The reddening $E(B-V)$ is found to be variable between 0.50 to 0.90 mag. Polarimetric and photometric results indicate for the presence of slightly bigger dust grains within the intra-cluster medium. Although our previous work (Eswaraiah et al. 2011) reveals uniform dust grain alignment in the foreground medium towards the direction of NGC 1931, the polarization efficiency is found to be less than that of the general diffuse interstellar medium. This could be due to the normal extinction law in the foreground medium and anomalous reddening law in the intra-cluster medium.

Keywords: Star formation, Open clusters, Photometry, Polarization, ISM dust and Magnetic fields
PACS: 97.10.Bt, 98.20.Di, 95.55.Qf, 98.35.Eg, 98.38.Cp,97.10.Ld,98.35.Ln

1. INTRODUCTION

Optical polarimetry is an efficient tool to study the properties of the dust and can provide vital information regarding orientation of the magnetic field towards the direction of star-forming regions. When un-polarized light passes through an ensemble of non-spherical dust grains aligned with respect to the Galactic magnetic field the light gets linearly polarized at the level of few percent. Dust distribution in the form of dust layers and the properties of dust grains, magnetic field orientation along the line of sight, nature of environment in which dust exist, nature of extinction laws along a particular line of sight etc are the important factors that can determine the dust grain polarization efficiency. The mechanism which responsible for the dust grain alignment is still an ongoing debate in the astronomical community, even though it is believed that the Davis-Greenstein mechanism (Davis & Greenstein 1951) could be responsible for the dust grain alignment, however recently, radiative torque alignment (Lazarian 2007; Lazarian & Hoang 2007; Andersson et al. 2011) attained much attention and seems to be a promising mechanism which can explain the dust grain alignment in all the environments such as diffuse ISM and molecular clouds etc.

Young star clusters which are still embedded in the parent molecular cloud, are unique laboratories to study the dust properties, the nature of interaction between young star(s) and the surrounding medium as well as to study the star formation scenario in the region. This paper is continuation of our efforts to understand the star formation scenario (Pandey et al. 2008, Sharma et al. 2007 & 2010, Jose et al. 2008 & 2011, Samal et al.

First International Conference on Chemical Evolution of Star Forming Region and Origin of Life
AIP Conf. Proc. 1543, 138-147 (2013); doi: 10.1063/1.4812608

2007 & 2010, Chauhan et al. 2009 & 2011a,b) and dust characteristics in star-forming regions as well as to map the structure of magnetic field at diverse environments of the Milky Way Galaxy (Eswaraiah et al. 2011 & 2012).

Here we report broad-band optical photometric and polarimetric observations around the cluster NGC 1931. NGC 1931 ($\alpha_{2000} = 05^h\ 31^m\ 25^s$, $\delta_{2000} = +34^\circ\ 14'\ 42''$; l=173.9°, b=0.28°) is a young star cluster associated with a gas-dust complex. The cluster is associated with the bright nebula Sh 2-237 in Auriga. The distance estimates for the cluster varies between 1.8 kpc to 3.1 kpc and the post-main-sequence age of the cluster is reported to be $\sim$ 10 Myr (Moffat et al. 1979, Pandey & Mahra 1986, Bhatt et al. 1994, Chen et al. 2004, Bonatto & Bica 2009). Glushkov, Denisyuk & Karyagina (1975) reported that Sh2-237 is excited by a star of spectral type B0.5. Leisawitz et al (1989) have found that the portion of Sh2-237 is obscured by a molecular cloud.

2. OBSERVATION & DATA REDUCTION

The CCD $UBV(RI)_c$ and Hα photometric data were acquired on 2005 December 31; 2006 January 22, 23; and 2006 Febraruy 24, using the 2048 $\times$ 2048 pixel CCD camera mounted on the $f/13$ Cassegrain focus of the 104-cm Sampurnanand Telescope of Aryabhatta Research Institute of Observational Sciences (ARIES), Nainital. The broad-band $UBV(RI)_c$ observations were standardized by observing stars in the SA98 field (Landolt 1992) on 23 January 2006. A blank field of $\sim$13$\times$13 arcmin^2 located at a distance of about 40 arcmin away towards north-west of the cluster was used to estimate the contamination due to foreground/background field stars.

Polarimetric observations were carried out on two nights (2010 November 12 and 2010 December 13), using the ARIES Imaging Polarimeter (AIMPOL; Rautela, Joshi & Pandey 2004) mounted at the Cassegrain focus of the 104-cm Sampurnanand telescope of the ARIES, Nainital, India. The details of the instrument, observation and data reduction can be found in Eswaraiah et al. (2011 & 2012).

3. RESULTS

3.1. Polarimetry: membership and Serkowski parameters (P_{max} and λ_{max})

Color-color diagram in combination with Q_V versus U_V Stokes plane can be used to identify the members of a cluster (cf. Eswaraiah et al. 2011). In the Stokes plane the Stokes parameters of cluster members should show a clustered distribution around the mean values of Q_V and U_V as the light from the cluster members is affected approximately by a similar column density of aligned dust grains. The dispersion from the mean values of the cluster members may be caused by various factors such as the variable reddening, variation in the dust properties and the variation in the physical conditions in the intra-cluster medium. The cluster members may also show scattered distribution in the Stokes plane because of the intrinsic polarization and/or rotation in the polarization angles due to circumstellar disks/envelopes around young stellar objects.

We have carried out multi-band polarimetric observations for 62 stars. Out of 62, 57 stars have V-band polarimetric measurements. The black vectors in Fig. 1 represent the sky projection of V-band polarization measurements for 57 stars drawn on the 2MASS K-band image. In the case of 5 stars V-band polarization measurements are not available, in those cases we plotted the polarization measurements either of R_C-band (red) or I_C-band (magenta). The length of each polarization vector is proportional to the degree of polarization. The dashed-dot line represents the orientation of the projection of the Galactic plane (*GP*) at $b = 0.30°$, which corresponds to a position angle of 142°. Interestingly, all the polarization vectors except those near the cluster center (enclosed by a square box) are closely aligned with the GP. The enlarged view of the central region is shown in a separate panel at the top right part of the figure.

The left panel of Fig 2 shows Q_V versus U_V diagram for the 57 stars with V-band polarization measurements. Whereas the right panel of Fig 2 is $(B-V)$ versus $(U-B)$ for 58 stars as the $(U-B)$ and $(B-V)$ colors are not available for 4 stars. The Gaussian fit to the V-band polarization measurements of 57 stars yields mean and standard deviation as $P_V = 2.4\pm0.6$ per cent and $\theta_V = 155°\pm7°$. These values have been used to plot the 1σ box in the left panel of Fig. 2. The values of mean P_V (2.4±0.6 per cent) and mean θ_V (155° ±7°) towards NGC 1931 are comparable to those (P_V=2.3±0.1 per cent and θ_V =160° ±3°, Eswaraiah et al. 2011) obtained for Stock 8 (l =173.37°, b=-0.18°, distance = 2.05 kpc) which is located near the NGC 1931. On the basis of star's position in both color-color and Stoke's diagram, we identified 22 cluster members. A few more probable PMS members in the cluster region were identified on the basis of NIR/MIR colour-colour diagram and optical/NIR color-magnitude diagram. The details can be found in the forthcoming paper.

Out of 22 probable members, 11 stars have either $\sigma_1 > 1.5$ and (or) $\overline{\varepsilon} > 2.3$ indicating the the presence of intrinsic polarization and/or rotation in their polarization angles. To study the dust properties (P_{max} and λ_{max}), we need to consider only those probable members which are free from either intrinsic polarization and (or) rotation in their polarization angles. The weighted mean values of P_{max} and λ_{max} using 11 stars, which do not show intrinsic polarization and (or) rotation in their polarization angles, are found to be 2.52±0.04 per cent and 0.57±0.02 μm, respectively. However the λ_{max} value (0.55±0.01μm; Eswaraiah et al. 2011) towards the cluster NGC 1893, which is spatially close to NGC 1931, is found to be comparable to the value for the diffuse ISM (0.545μm; Serkowski et al. 1975) as well as the reddening law is found to be normal (Sharma et al. 2007). This indicates that size of the dust grains is comparable to those in the diffuse ISM. Jose et al. (2008) have also found the presence of normal reddening law in the cluster region of Stock 8 which is also located near the NGC 1931. The indication of slightly bigger dust grains towards NGC 1931 could be due to slightly bigger dust grains within the "intra-cluster medium".

3.2. Extinction law

The TCDs of the form of $(V-\lambda)$ vs. $(B-V)$, where λ is one of the wavelengths of the broadband filters R, I, J, H, K or L, can used to separate the influence of the

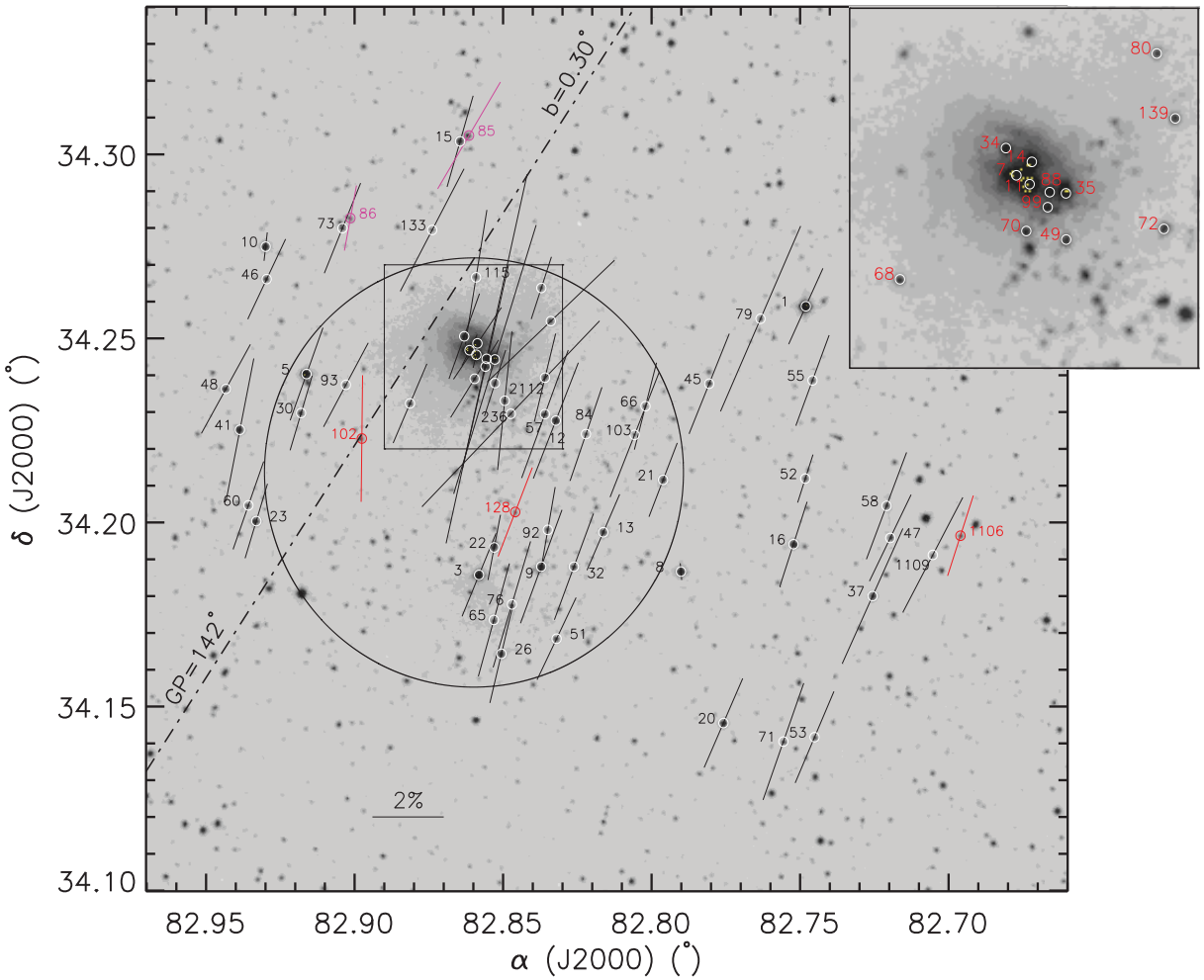

FIGURE 1. The polarization measurements of the stars in NGC 1931 are over plotted in 2MASS K_s-band image. The stars with V-band polarimetric measurements are shown with black vectors. The red and magenta vectors represent polarimetric measurements in R_C and I_C-bands. The position angle corresponding to the $b = 0.30°$ (GP) is also shown at 142° with a dot-dashed line. A vector with a 2 per cent of polarization at a position angle of 90° is drawn for a reference. Barring a few vectors near the cluster center (shown in a square box), majority of the vectors are closely aligned with GP indicating an ordered magnetic field towards NGC 1931. The vectors in the nebulous region of the cluster show rather scattered distribution. The box at the corner shows an enlarged view of the central region.

normal extinction produced by the diffuse ISM from that of the abnormal extinction arising within the cluster region having a peculiar distribution of dust sizes (cf. Chini & Wargau, 1990; Pandey et al., 2000). The $(V-\lambda)$ vs. $(B-V)$ TCDs for the probable members and probable PMS stars of the cluster region are shown in Fig. 3. The open circles are the stars with $V(RI)_C$ polarimetric data and the triangles are those with either single or double band polarimetric data. The slope for the general distribution of majority of the stars (excluding the stars in the nebulous region shown with filled square symbols and two PMS stars # 88 and 236) is found to be 1.17±0.05, 2.10±0.12, 2.63±0.14 and 2.76±0.16 for $(V-I)$, $(V-J)$, $(V-H)$, $(V-K)$ versus $(B-V)$ TCDs

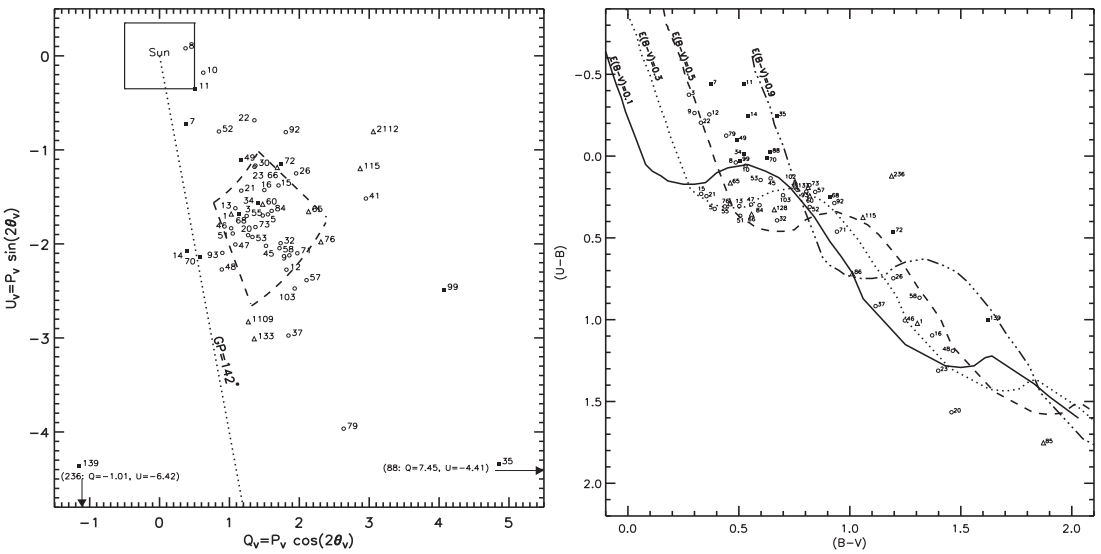

FIGURE 2. (Left panel) U versus Q diagrams for 57 stars observed in V-band. Open circles represent the stars having V-band data. The filled squares represent the stars located within the box at the cluster center. The triangles represent the stars having either single or double band polarimetric data. The box with dashed line marks the boundary of mean $P \pm \sigma$=2.4±0.6 per cent and mean $\theta \pm \sigma$=155°±7°. The position of the Sun is also shown with a square box at the (Q=0, U=0) coordinates. The GP is drawn with a dotted line. The stars distributed within or nearby 1σ box of all the three Stoke's planes could be probable members associated with the cluster.(Right panel): $(U-B)$ versus $(B-V)$ TCD of the stars with polarimetric data. The symbols same as in left panel. The zero-age main sequence (ZAMS) from Schmidt-Kaler (1982) is shifted along a normal reddening vector having a slope of $E(U-B)/E(B-V)$ = 0.72. The TCD shows a variable reddening in the cluster region with $E(B-V)_{min} \sim 0.5$ mag and $E(B-V)_{max} \sim 0.9$ mag.

respectively. These slopes are higher in comparison to those obtained for normal ISM, which indicates an anomalous reddening law in the cluster region. The stars associated with the nebulous region of northern cluster, shown with filled square symbols, seem to be deviating from the distribution of majority of the stars. Hence, both our polarimetric and photometric results indicate for the presence of anomalous reddening law towards NGC 1931 indicating the presence of slightly bigger dust grains within the intra-cluster medium.

3.3. Polarization efficiency

The ratio of $P_{max}/E(B-V)$ is known to be a measure of the polarization efficiency of the ISM and it depends mainly on the grain alignment efficiency, the magnetic field strength and the amount of depolarization due to the radiation traversing diffuse clouds with different magnetic field directions (see e.g. Feinstein et al. 2003; Orsatti et al. 2003; Martínez et al. 2004; Vergne et al. 2007, 2010; Eswaraiah et al. 2011 & 2012). Figure 4 displays the polarization efficiency diagram for 11 probable cluster members without intrinsic polarization and two foreground stars. It is well known that for the

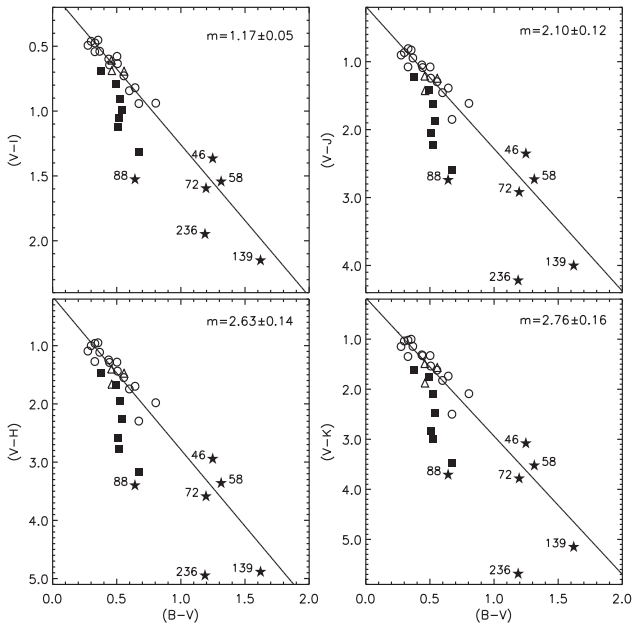

FIGURE 3. The TCDs of the form $(V-\lambda)$ vs. $(B-V)$, where λ is I, J, H or K_s. Only the probable cluster members identified on the basis of polarimetric data, photometric color-color diagrams and colour-magnitude diagram have been used. The open cirlces and triangles represent the stars having $V(RI)_C$ and single or double band polarimetric data, respectively. The star symbols are the probable PMS stars. The filled squares symbols are the stars lying in the cluster center shown by a square box in the Fig. 1. The straight line fit values are indicated on right hand side of each panel. The stars in the nebulous region (filled square symbols) and two (# 88 and 236) PMS stars are not used in the fit.

diffuse ISM the polarization efficiency cannot exceed the empirical upper limit given by, $P_{max} = 3A_V \simeq 3R_V E(B-V) \simeq 9.3E(B-V)$ per cent (assuming R_V =3.1, Hiltner & Johnson, 1956; Serkowski et al., 1975) and the same is shown by a continuous line in Fig. 4. For the average ISM, Serkowski et al. (1975) have found that the polarization efficiency of the ISM follows a mean relation $P_{max} \simeq 5E(B-V)$, which is shown by a dashed line. The recent estimate of the average polarization efficiency for the general diffuse ISM by Fosalba et al. (2002), which is valid for $E(B-V) < 1.0$ mag, is shown with a dashed-dot line.

Reddening values of individual probable 11 member stars having spectral types earlier than A0 has been computed by means of the reddening free index Q (Johnson & Morgan, 1953). Assuming a normal reddening law we have constructed a reddening-free parameter index Q = $(U-B) - 0.72(B-V)$. For the MS stars, the intrinsic $(B-V)_0$ color and color-excess can be obtained from the relation $(B-V)_0 = 0.332\times$Q (Johnson, 1966; Hillenbrand et al., 1993) and $E(B-V) = (B-V) - (B-V)_0$, respectively. The reddening values for the foreground stars (#8 and #10) have also been estimated. Figure 4 shows that star #99 has relatively high polarization ($P_{max} \sim 5.2$ per cent) and polarization efficiency greater than 5 per cent per mag. However, the majority of the cluster members are distributed below the dashed line indicating that the intracluster medium exhibits less polarization efficiency than the mean value for the diffuse ISM ($\sim$5 per cent per mag) and seems to follow the relation for the general diffuse ISM by Fosalba et al. (2002).

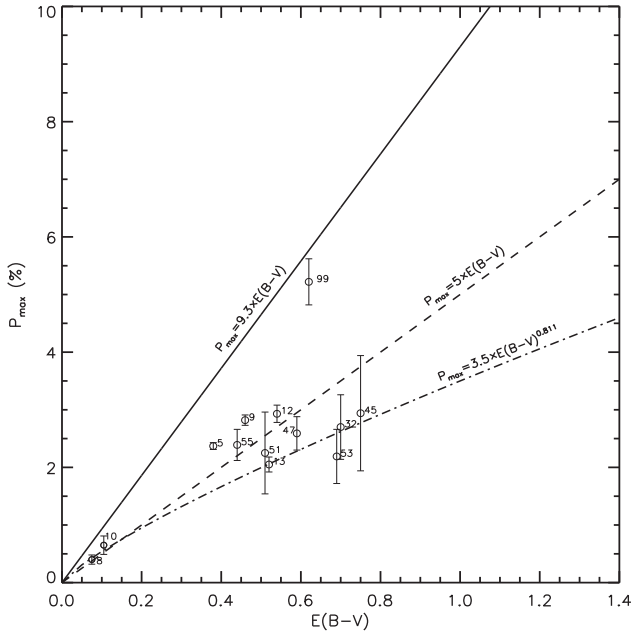

FIGURE 4. P_{max} versus $E(B-V)$ diagram for the 11 confirmed probable members and 2 confirmed foreground stars (#8 and #10) that are free from intrinsic polarization and (or) rotation in their polarization angles. The continuous line represents the empirical upper limit relation for the polarization efficiency (assuming R_V= 3.1) of $P_{max} = 9.3 \times E(B-V)$ (Serkowski et al 1975). The dashed line represents the relation $P_{max} = 5 \times E(B-V)$ (Serkowski et al 1975) and the dot-dashed line represents the relation P_{max} = 3.5 $\times$ $E(B-V)^{0.8}$ by Fosalba et al. (2002).

The observed less polarization efficiency could be because of the presence of normal sized dust grains in the foreground medium with normal reddening law and the presence of slightly bigger dust grains within the intra-cluster medium with anomalous reddening law.

3.4. Distance

The $V_0/(B-V)_0$ color magnitude diagram of the 22 probable identified members has been used to estimate the distance to the cluster. A visual fit of the isochrone for 1 Myr and Z=0.02 by Marigo et al. (2008) to the observations yield a distance modulus of $V_0 - M_V$=11.81$\pm$0.3 which corresponds to a distance of 2.3$\pm$0.3 kpc. The distance estimate is in agreement with that obtained by Pandey & Mahra (1986); Bhatt et al. (1994); Bonatto & Bica (2009).

3.5. Structure of the cluster

The initial stellar distribution in star clusters may be governed by the structure of parental molecular cloud as well as how star formation proceeds in the cloud (Chen

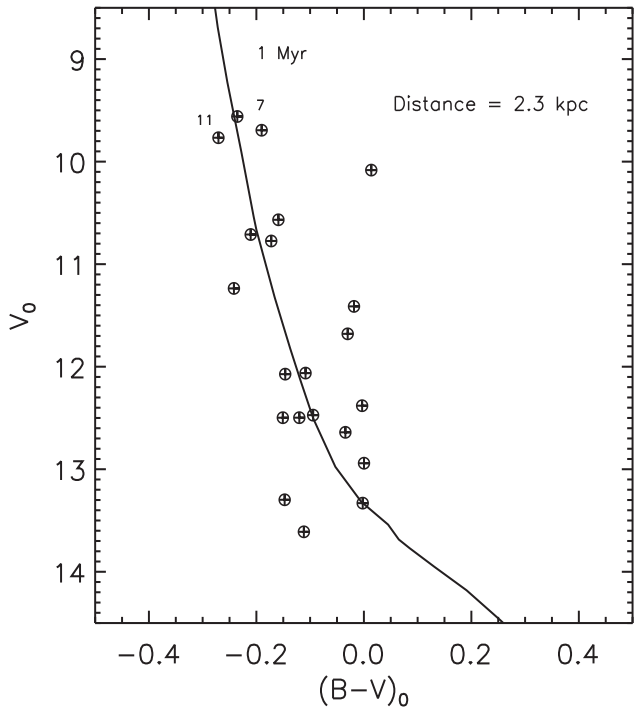

FIGURE 5. De-reddened V versus $(B-V)$ color-magnitude diagram for 22 probable members stars. The post main-sequence isochrones for 1 Myr (Z=0.02) by Marigo et al. (2008) has been plotted after correcting for the distance and reddening.

et al., 2004; Sharma et al., 2006). Later evolution of the cluster may be governed by internal gravitational interaction among member stars and external tidal forces due to the Galactic disc or giant molecular clouds.

To study the morphology of the cluster, we generated isodensity contours for the stars detected in 2MASS K_s-band and are shown in Fig. 6. The contours are plotted above 1σ level. The surface density distribution reveals two prominent structures clusterings around $\alpha(2000)$ $=05^h31^m25^s$, $\delta(2000)$ $=+34^\circ14'28''$ and $\alpha(2000)$ $=05^h31^m22^s$, δ (2000) $=+34^\circ10'44''$, suggesting the presence of a double cluster in the region. In fact the radial density profile (RDP) of the region by Bonatto & Bica (2009) also reveals a density enhancement around the radial distance of $\sim$ 3–5 arcmin.

4. CONCLUSIONS

In this study we have further shown that the polarization measurements in combination with the $(U-B)-(B-V)$ colour-colour diagram provide a better identification of the cluster members. The estimated distance of 2.3$\pm$0.2 kpc to the cluster is in agreement with the values obtained by us in previous studies. The interstellar extinction in the cluster region is found to be variable with $E(B-V)_{min} \simeq 0.5$ mag, $E(B-V)_{max} \simeq$ 0.9 mag. The polarimetric as well as photometric studies both indicate that the ratio of total-to-selective extinction in the cluster region, $R_{cluster}$, could be higher than the

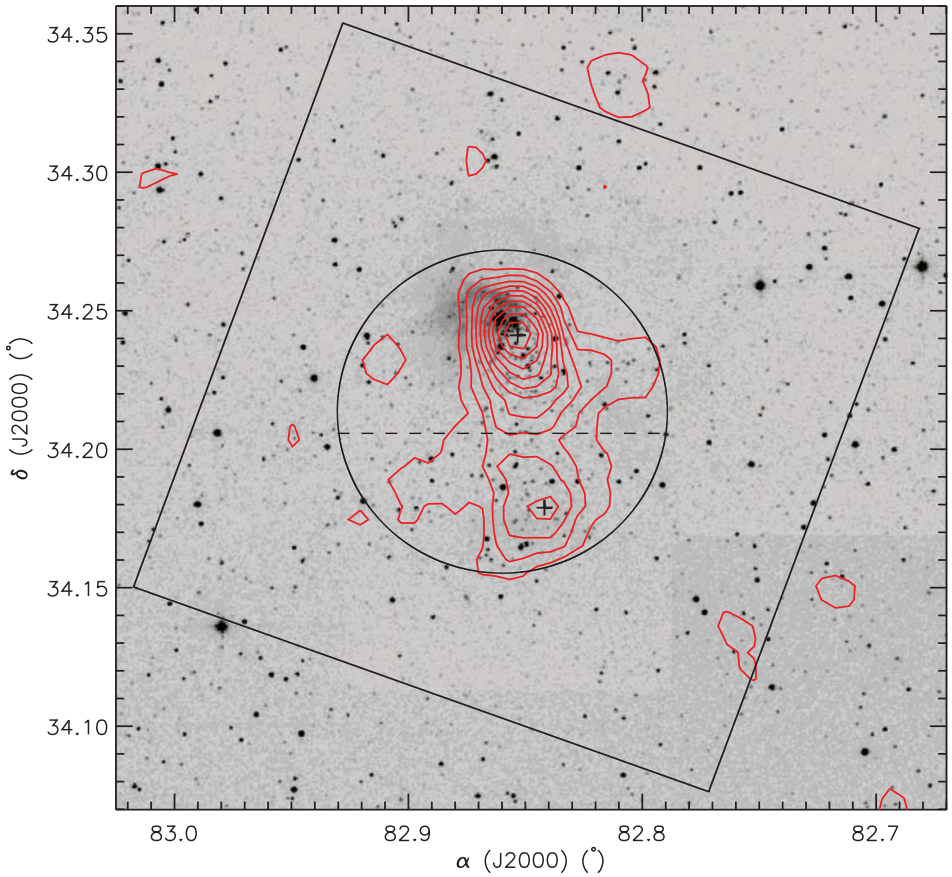

FIGURE 6. The isodensity contours generated from the 2MASS K_s-band data (with $\sigma_{K_s} < 0.1$ mag) using a grid size of $\simeq$35 $\times$ 35 arcsec^2. The contours are plotted above 1σ level. The contours have step size of 2 stars/arcmin^2 with the lowest contour representing 5 stars/arcmin^2. Isodensity contours manifest two prominent clustering. The dashed line demarcates northern and southern parts of the region. The area marked with continuous line represents the region covered by optical photometry. The circle represents estimated boundary of the region. The plus sign represents the center of the clusters.

normal which indicates an anomalous reddening law in the region. The polarization efficiency towards the NGC 1931 region is significantly smaller as compared to that towards NGC 1893, which is located spatially near to the NGC 1931. The stellar density distribution in the region reveals two separate clusterings. The radial extent of the region is estimated to be $\sim$3.5 arcmin.

ACKNOWLEDGMENTS

Authors are thankful to the GITA/DST (India) and NSC (Taiwan) for the financial support to carry out this work.

REFERENCES

1. Andersson, B.-G., Pintado, O., Potter, S. B., Straižys, V., & Charcos-Llorens, M. 2011, A&A, 534, A19
2. Bhatt, B. C., Pandey, A. K., Mahra, H. S., & Paliwal, D. C. 1994, Bulletin of the Astronomical Society of India, 22, 291
3. Bonatto, C., & Bica, E. 2009, MNRAS, 397, 1915
4. Chauhan, N., Ogura, K., Pandey, A. K., Samal, M. R., & Bhatt, B. C. 2011b, PASJ, 63, 795
5. Chauhan, N., Pandey, A. K., Ogura, K., et al. 2009, MNRAS, 396, 964
6. Chauhan, N., Pandey, A. K., Ogura, K., et al. 2011a, MNRAS, 415, 1202
7. Chen, W. P., Chen, C. W., & Shu, C. G. 2004, AJ, 128, 2306
8. Chini, R., & Wargau, W. F. 1990, A&A, 227, 213
9. Davis, L., Jr., & Greenstein, J. L. 1951, ApJ, 114, 206
10. Eswaraiah, C., Pandey, A. K., Maheswar, G., et al. 2011, MNRAS, 411, 1418
11. Eswaraiah, C., Pandey, A. K., Maheswar, G., et al. 2012, MNRAS, 419, 2587
12. Feinstein, C., Martínez, R., Vergne, M. M., Baume, G., & Vázquez, R. 2003, ApJ, 598, 349
13. Fosalba, P., Lazarian, A., Prunet, S., & Tauber, J. A. 2002, ApJ, 564, 762
14. Glushkov, Y. I., Denisyuk, E. K., & Karyagina, Z. V. 1975, A&A, 39, 481
15. Hillenbrand, L. A., Massey, P., Strom, S. E., & Merrill, K. M. 1993, AJ, 106, 1906
16. Hiltner, W. A., & Johnson, H. L. 1956, ApJ, 124, 367
17. Johnson, H. L. 1966, ARA&A, 4, 193
18. Johnson, H. L., & Morgan, W. W. 1953, ApJ, 117, 313
19. Jose, J., Pandey, A. K., Ogura, K., et al. 2011, MNRAS, 411, 2530
20. Jose, J., Pandey, A. K., Ojha, D. K., et al. 2008, MNRAS, 384, 1675
21. Lazarian, A. 2007, JQSRT, 106, 225
22. Lazarian, A., & Hoang, T. 2007, MNRAS, 378, 910
23. Leisawitz, D., Bash, F. N., & Thaddeus, P. 1989, ApJS, 70, 731
24. Marigo, P., Girardi, L., Bressan, A., et al. 2008, A&A, 482, 883
25. Martínez, R., Vergne, M. M., & Feinstein, C. 2004, A&A, 419, 965
26. Moffat, A. F. J., Jackson, P. D., & Fitzgerald, M. P. 1979, A&AS, 38, 197
27. Orsatti, A. M., Vega, E. I., & Marraco, H. G. 2003, A&A, 408, 135
28. Pandey, A. K., & Mahra, H. S. 1986, Ap&SS, 120, 107
29. Pandey, A. K., Ogura, K., & Sekiguchi, K. 2000, PASJ, 52, 847
30. Pandey, A. K., Sharma, S., Ogura, K., et al. 2008, MNRAS, 383, 1241
31. Rautela, B. S., Joshi, G. C., & Pandey, J. C. 2004, Bulletin of the Astronomical Society of India, 32, 159
32. Samal, M. R., Pandey, A. K., Ojha, D. K., et al. 2007, ApJ, 671, 555
33. Samal, M. R., Pandey, A. K., Ojha, D. K., et al. 2010, ApJ,714, 1015
34. Schmidt-Kaler Th., 1982, in Schaifers K., Voigt H. H., Landolt H., eds, Landolt-Bornstein, Vol. 2b. Springer, Berlin, p. 19
35. Serkowski, K., Mathewson, D. S., & Ford, V. L. 1975, ApJ, 196, 261
36. Sharma, S., Borissova, J., Kurtev, R., Ivanov, V. D., & Geisler, D. 2010, AJ, 139, 878
37. Sharma, S., Pandey, A. K., Ogura, K., et al. 2006, AJ, 132, 1669
38. Sharma, S., Pandey, A. K., Ojha, D. K., et al. 2007, MNRAS, 380, 1141
39. Vergne, M. M., Feinstein, C., & Martínez, R. 2007, A&A, 462, 621
40. Vergne, M. M., Feinstein, C., Martínez, R., Orsatti, A. M., & Alvarez, M. P. 2010, MNRAS, 403, 2041